Lens Aberration Aware Placement for Timing Yield

Andrew B. Kahng   Chul-Hong Park   Puneet Sharma   Qinke Wang

Abstract

Process variations due to lens aberrations are to a large extent systematic, and can be modeled for purposes of analyses and optimizations in the design phase. Traditionally, variations induced by lens aberrations have been considered random due to their small extent. However, as process margins reduce, and as improvements in reticle enhancement techniques control variations due to other sources with increased efficacy, lens aberration-induced variations gain importance. For example, our experiments indicate that lens aberration can result in up to 8% variation in cell delay. Aberration-induced variations are systematic and depend on the location in the lens field. In this paper, we propose an aberration-aware timing-driven analytical placement approach that accounts for aberration-induced variations during placement. Our approach minimizes the design's cycle time and prevents hold-time violations under systematic aberration-induced variations. On average, the proposed placement technique reduces cycle time by $\sim 5\%$ at the cost of $\sim 2\%$ increase in wirelength.

I. Introduction

Low *k*-factor lithography drives many new process-design interactions that must be comprehended early in the development process to ensure rapid yield ramp-up and acceptable steady-state yield entitlement. Modern lithography tools can image a complex chip pattern with billions of pixels, within an exposure time of a fraction of a second. However, all optical projection systems used for microlithography depart from perfection because of various lens aberrations, especially when large image field size is combined with high numerical aperture (NA).

Aberrations can be described as the departure from ideal imaging induced by an imperfect lens system, as shown in Figure 1. Aberrations cause optical path differences among the rays, resulting in wavefront deviation from a reference sphere at the exit pupil; this induces blur and distortion of images. Undesirable imaging artifacts from aberration are uncorrectable and, indeed, are sometimes exacerbated through use of resolution enhancement techniques (RETs) such as phase-shift mask and off-axis illumination [1]. The effects of lens aberrations on lithographic imaging [7] [29] include shifts in the image position, image asymmetry, reduction of the process window, and the appearance of undesirable imaging artifacts. *Zernike's coefficients* capture the deviation from ideal imaging and may be used during lithography simulation to predict the impact of lens aberration on critical dimension (CD). CD variation caused by lens aberration is relatively small compared to that caused by defocus and pattern proximity. However, most CD error caused by proximity *can* be corrected by RETs. Thus, lens aberration has turned out to be a major source of residual errors in across-field linewidth variation (AFLV) [5].

A preliminary version of this work appeared in [10].

A. B. Kahng is with the Departments of Computer Science and Engineering, and of Electrical and Computer Engineering, University of California at San Diego, La Jolla, CA 92093-0404. E-mail: abk@ucsd.edu.

C.-H. Park and P. Sharma are with the Department of Electrical and Computer Engineering, University of California at San Diego, La Jolla, CA 92093-0409. E-mail: chpark@vlsicad.ucsd.edu, sharma@ucsd.edu.

Q. Wang is with the Department of Computer Science and Engineering, University of California at San Diego, La Jolla, CA 92093-0114. E-mail: qiwang@cs.ucsd.edu.

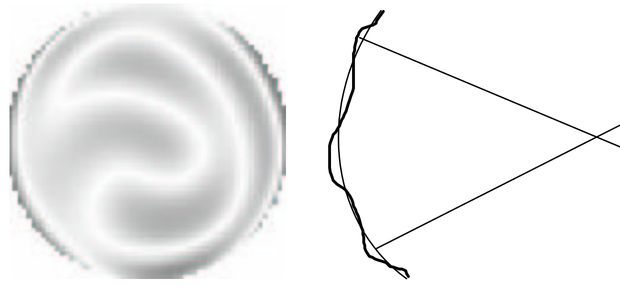

Fig. 1. An imperfect lens system.

Recent studies of lens aberration control have focused on measurement systems [28] [6] and pattern sensitivity of aberration [31], as well as lens mounting systems to compensate for the aberration [19]. However, despite these efforts, the impact of lens aberration on CD will be an ever-present barrier to manufacturing yield as minimum design rules are pushed ever closer to fundamental resolution limits. From the design perspective, variations in CD affect the delays, slews, input capacitances and leakage of a given logic cell. We also observe that the maximum difference in delays of all timing arcs in a cell (delay skew) increases significantly due to lens aberration as different MOS devices in the layout are affected differently by aberration.

Progler et al. [22] studied the impact of lens aberration on statistical timing behavior and observed that certain aberration coefficients are associated with large timing error. Orshansky et al. [23] found that spatial gate CD variation leads to a large variation in the raw speed of CMOS logic. Misleading timing results are obtained, which lead to slower and/or malfunctioning circuits because the simulation of a circuit's behavior has ignored the spatial CD information. The systematic variability of gate CD caused by lens aberration can be modeled in order to achieve better performance by way of accurate timing analysis at all stages of physical implementation [25], [26]. However, more accurate analysis of gate delay impact has been required as the scaling of lithographic features makes the lens aberrations even more complex. In this paper, we first describe a novel aberration-aware static timing analysis flow that integrates (i) results of lithography simulation to measure CD across the lens field, (ii) SPICE simulation-based library performance characterization that captures variant CD combinations in library cell instances, and (iii) placement information.

We also propose an aberration-aware timing-driven analytical placement framework that utilizes the aberration-aware timing analysis flow to minimize clock cycle time and avoid hold-time violations, without significantly increasing total wirelength. The placer is driven by models that capture the impact of lens position on timing arc delays in cells, and by weighted-wirelength models. Essentially, we preferentially place cells that are setup-time (resp. hold-time) critical at lens field locations where aberrations cause the cell delay to decrease (resp. increase).

The contributions of our work are as follows.

- Using industry OPC recipes, aberration parameters, and design testcases, we show that the variation in timing due to lens aberration can be significant. Over the cells in a 90nm foundry library, we observe cell delay (averaged over all timing arcs) to change by $2\% - 8\%$. The maximum difference in delays of all timing arc of a cell (*delay skew*) increases significantly.
- We develop a novel aberration-aware timing analysis flow that affords more accurate timing analysis, taking into

account the position of the chip in the lens field. It also considers the increase in delay skew caused by aberration.

- We propose an aberration-aware, timing-driven analytical placement flow that considers the impact of lens aberrations on timing to minimize clock period and avoid hold-time violations without significant total wirelength increase. Averaged over our testcases, worst-case cycle time reduces by $\sim 5\%$ at the cost of $\sim 2\%$ increase in wirelength, and there are no hold-time violations.

The remainder of this paper is organized as follows. In Section 2, we describe lens aberration and study its impact on CD and gate delay. Section 3 proposes a novel aberration-aware timing analysis and the accompanying flow. Section 4 describes our aberration-aware analytical placement formulation and implementation details. Test designs, experimental conditions and experimental results are described in Section 5. We conclude in Section 6 with directions for ongoing research.

II. Design Impact of Lens Aberration

In this section we briefly describe how lens aberration impacts CD and consequently circuit delay.

A. CD impact of Lens Aberration

Several manufacturing process steps are involved in transfer of the pattern on the mask to the photoresist, and then to the wafer. Lens aberration comes into play when the photoresist is exposed to light during lithography. Broadly speaking, a lithography setup includes one or more illumination sources, a mask, several lenses, and photoresist applied to the wafer. Modern lithography systems use step-and-scan to expose small portions of the wafer at a time, and then shift to the next region. The portion of the wafer that gets exposed in a step is called the *lens field*, or simply *field*. In each step, the photoresist is exposed to light through a slit that is scanned from one side of the field to the other [32].

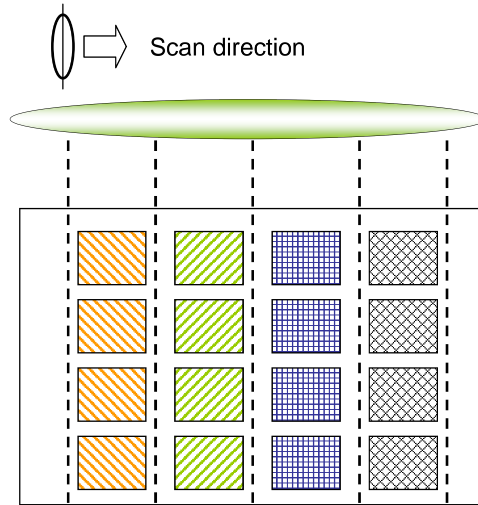

Fig. 2. Different CD qualities of chips in a reticle due to aberration across the lens field.

Lens aberration parameters (Zernike's coefficients), which capture the divergence from ideal behavior of light, change as the slit translates horizontally. *Hence, the CD error induced by lens aberration varies along the horizontal*

direction but stays constant along the vertical direction. While the variation in CD along the horizontal direction is continuous, it is reasonable to discretize it and assume it to remain constant over small regions as shown in Figure 2. Based on industry-supplied Zernike's coefficients at multiple locations in the lens field, we run lithography simulation on some frequently-used standard cells from a 90nm foundry library, and study the impact on CD. Figure 3 shows average CD variation of devices in BUFX4, INVX2, NAND2X4 and NOR2X1 cell instances as their position within the lens field is varied. For example, average gate CD variation of NAND2X4 at 100nm worst defocus is up to 8nm across the entire lens field. In addition, we investigate the *CD skew* (maximum difference in CD over all devices in a cell) of different cells. Large CD skew can unbalance the timing arcs of a cell, as we discuss in greater detail in Section 3. Figure 4 shows the CD skew for NAND2X4 as its position in the lens field is changed. It is evident from these studies that the aberration impact on CD error is large across the lens field, and must be modeled to reduce guardbanding and overdesign.

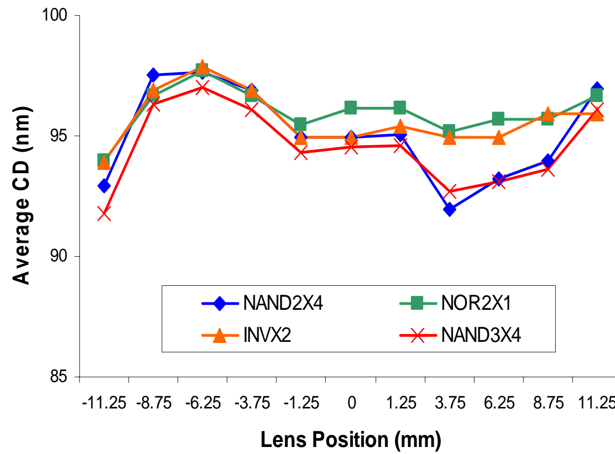

Fig. 3. Average gate CD varies accross the lens field; the range of this variation for the NAND2X4 cell is 8nm.

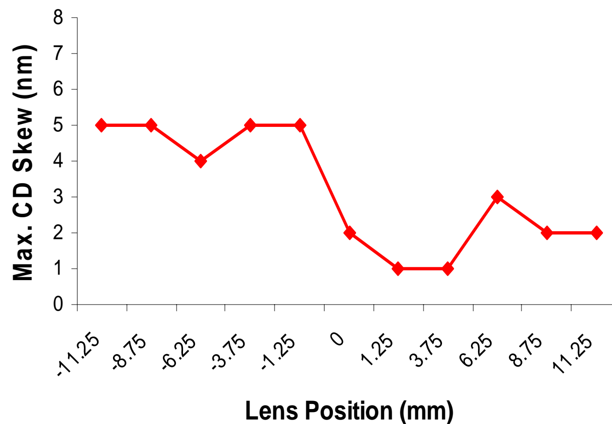

Fig. 4. Maximum CD skew among all gates in NAND2X4 cell.

B. Delay Impact of Lens Aberration

Variations in CD directly and indirectly affect circuit delay. At the device level, increase in gate CD causes an approximately linear decrease in saturation on-current of the device which partially determines its delay. Since lens aberration affects different devices in a cell differently, each of the cell's timing arcs can be affected differently. Most standard cells are designed such that the maximum difference in delays of timing arcs (*delay skew*) is small. Due to lens aberration, however, this delay skew can increase - i.e., arcs that are governed by larger-than-nominal CDs will be slowed down, while those governed by smaller-than-nominal CDs will be sped up. Figure 5 shows how the delay, averaged over all timing arcs, changes for four cell masters as the cell instance location is varied from the lens center. Figure 6 shows the aberration-induced increase in delay skew with respect to the delay skew of the nominal (or drawn) cell as the location of cell NAND2X4 is varied in the field.

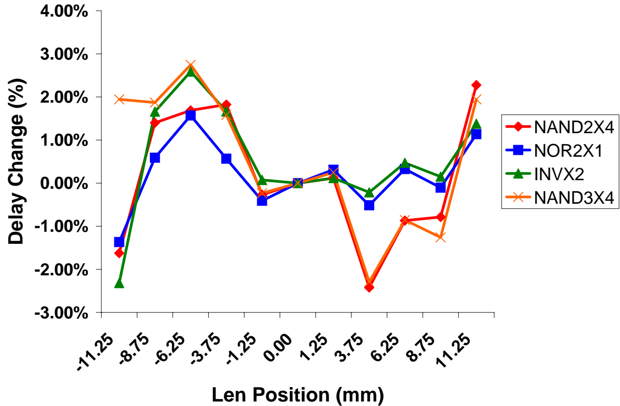

Fig. 5. Change in average delay with lens position with respect to center of the lens.

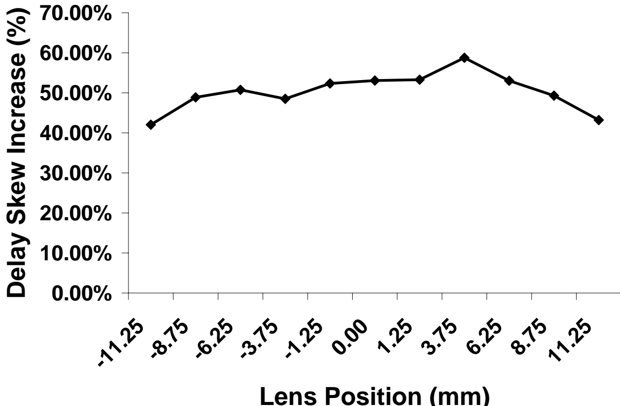

Fig. 6. Percentage increase in delay skew (maximum difference in delays of all timing arcs) of the NAND2X4 cell as lens position is changed, relative to the maximum delay skew of nominal (or drawn) cell. The increase is always over 40% because for computation of nominal delay skew, library characterization applies an equal CD error to all devices at worst-case process conditions. To compute aberration-induced delay skew, however, lithography simulation is performed at the worst-case process corner and all devices get different CD errors.

CD variations also cause variations in cell input capacitance and output slews (transition times). Input capacitance affects the loading of fanin cells and consequently their delays; interconnect delays are also affected. Similarly,

slews affect the output slews and delays of cells in the fanout cone. Again, to avoid unnecessary guardbanding, the performance analysis flow (library model characterization, timing/SI analysis, etc.) must comprehend these systematic variations.

III. Aberration-Aware Timing Analysis

In this section we describe our aberration-aware timing analysis flow. While the flow is complete and self-contained, it is at the same time designed for, and will be used by, the analytical placement framework described in Section 4. Our aberration-aware timing analysis flow involves two main steps: (1) constructing timing libraries of all standard cells for different locations in the lens field, and (2) using placement information of the design to compute the location of all cell instances in the lens field, then using this location information to look up appropriate models in the timing library for use with off-the-shelf static timing analysis (STA) tools.

Before describing our analysis flow, we describe two alternative flows and our reasons for not using them. In the first alternative flow, variants of each cell are created such that the CD of all devices in the cell is different for each variant, but the same for all devices in a given variant. A timing library can be created using SPICE models for all the variants. Since all devices in a cell variant have the same CD, we call this library a *cell-level* granularity library. To perform timing analysis on a placed design, lithography simulation is performed to obtain CDs of all devices in all cells. For each cell, the CDs of its devices can be averaged, and the closest-matching available cell variant in the timing library then fed to off-the-shelf STA. However, as CD skews can be large, averaging of device CDs can introduce inaccuracy the estimated impact of aberration. In other words, the effect of non-uniform CDs is non-uniformity in timing arc delays, rather than average increase or decrease in the delays of all timing arcs. Our experiments have found that the cell-level library-based approach is very inaccurate compared to the approach that we adopt.

The second alternative flow creates *a priori* variants for each cell master, such that there is one variant for every possible assignment of CDs to devices. This means that given any assignment of CDs to devices, an exactly matching, pre-characterized cell variant can be found. After lithography simulation provides CDs of all devices in all cells, a correctly matching variant can be picked for use in timing analysis. Though this flow is very accurate, it requires a very large number of cell variants (exponential in the number of devices in the cell); this is infeasible with respect to both characterization time and library size.

In our proposed flow, variants are created for each cell for different lens field locations. Figure 7 illustrates our timing library construction flow. We begin with standard-cell GDSII files and use *Mentor Graphics Calibre v9.3_5.11* for sub-resolution assist feature (SRAF) generation and model-based OPC. We use Zernike's coefficients for eight sampling positions in the lens field from a major chip maker, and compute the other coefficients at 19 different locations with 1.5mm stepsize on the field using linear interpolation. Using the post-OPC standard-cell GDSIIs and Zernike's coefficients, we perform lithography simulation at 19 different field locations with wavelength λ = 193, numerical aperture NA = 0.75, and annular aperture $\sigma = 0.75/0.50$. After lithography simulation, we have 19 PrintImage GDSII results for each standard cell; we then measure the CD of each of the MOS devices in each GDSII result.

Figure 8(a) shows the PrintImage contour generated by *Mentor Graphics PrintImage* for one device[1]. To measure

[1] Mentor Graphics PrintImage produces rectilinear contours; our approach, however, is generic enough to be used for arbitrary polygonal contours.

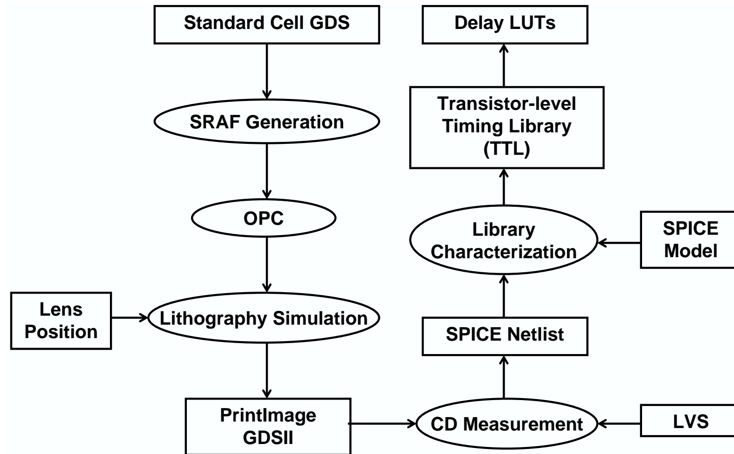

Fig. 7. Aberration-aware timing analysis and its flow.

the CD of the PrintImage contours, we first take an intersection with the active layer to obtain the contour of the gate. Contours are rectilinearized and split into rectangles in a staircasing fashion. The lengths of all rectangles are then averaged with rectangle widths as weights to compute the CD of the gate (i.e., $CD_{gate} = \sum^n l_i \times w_i / \sum^n w_i$ where n is the number of rectangles into which the contour is split, and l_i and w_i are the lengths and widths of the ith rectangle).

The measured CDs are then used to alter SPICE netlists of standard cells, preparatory to running library characterization. A complication arises because GDSII typically does not have device names, but SPICE netlists only reference devices by device names. We solve this problem by applying LVS (layout vs. schematic) to obtain a mapping between device locations and device names. After modifying the SPICE netlists, we run *Cadence SignalStorm* v4.1 to perform library characterization. Since lens aberrations affect different devices in a cell differently, the altered SPICE netlists may no longer have equal CD for all devices. We call our characterized library a *transistor-level timing library* (TTL); it accurately captures the delay skew induced due to CD skew while adding manageable complexity to the characterization effort and library size.

Our test library contains 50 combinational cells. For each we create 19 variants corresponding to 19 field locations. Library characterization requires approximately 6 hours (wall time) running on 18 CPUs ranging from *Intel Xeon 1.4GHz* to *AMD Opteron 2.2GHz*. We do not create variants for the 13 sequential cells in our library due to large CPU time (estimated at 60 hours on our machines) required by their characterization. We note that the characterization time can be significant but is a one-time task for each process.

IV. Aberration-Aware Timing-Driven Placement

Because of lens aberrations, a cell placed at different locations within the reticle will exhibit varying performance characteristics. In order to improve timing yield after manufacturing, we propose a lens aberration aware timing-driven placement formulation that minimizes total timing-weighted delays of cells in conjunction with common timing-driven placement objectives such as minimizing total timing-weighted wirelength. We implement our method based on a general analytical placement framework and describe implementation details in this section.

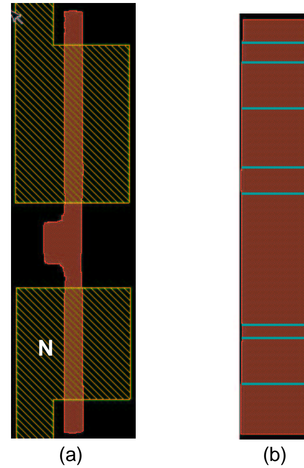

Fig. 8. Polygon generation for CD measurement: (a) result of PrintImage simulation of an inverter, and (b) rectilinearized polygon representation of a gate device in the region N of (a).

A. Introduction of Analytical Placement

Analytical placement methods have recently received increased attention from both academia and industry [3], [4], [9], [13], [20], [30]. Specifically, recent work has implemented *APlace*, a general analytic placement framework [11], [13], [14], [15], which has high solution quality and strong extensibility. Here we briefly introduce the APlace analytic placement framework, upon which we build our proposed aberration-aware timing-driven placement method.

APlace formulates global placement as a *constrained nonlinear optimization problem*: the layout area is uniformly divided into global cells and APlace minimizes total half-perimeter wirelength (HPWL) while maintaining an equalized cell area in each global bin (i.e., uniform density). A formal problem formulation is as follows:

$$\begin{aligned} &min \quad HPWL(\mathbf{x},\mathbf{y}) \\ &s.t. \quad D_g(\mathbf{x},\mathbf{y}) = D \quad \text{for each global cell } g \end{aligned} \tag{1}$$

where $(\mathbf{x},\mathbf{y})$ is the vector of center coordinates of cells, $HPWL(\mathbf{x},\mathbf{y})$ is the total HPWL of the current placement, $D_g(\mathbf{x},\mathbf{y})$ is a density function that equals the total cell area in a global bin g, and D is the average cell area over all global bins.

APlace applies smooth approximations of the HPWL and density functions and solves the constrained optimization problem in Eqn. (1) using the simple *quadratic penalty method*. I.e., the placer solves a sequence of unconstrained minimization problems of the form

$$min \quad HPWL(\mathbf{x},\mathbf{y}) + \tfrac{1}{2\mu}\textstyle\sum_g (D_g(\mathbf{x},\mathbf{y}) - D)^2 \tag{2}$$

for a sequence of values $\mu = \mu_k \rightarrow 0$ and use the solution of the previous unconstrained problem as an initial guess for the next one. A *Conjugate Gradient* (CG) solver is employed to optimize for the objective function in Eqn. (2). The conjugate gradient method is quite useful in finding an unconstrained minimum of a high-dimensional function. Also, the memory required is only linear in the problem size, which makes the approach adaptable to large-scale placement problems.

The general APlace framework has been extended to address a variety of placement tasks across many aspects of physical implementation, including mixed-size placement, timing-driven placement, power-aware placement, voltage-drop aware placement and I/O-core co-placement; it has been shown to be competitive in a wide variety of contexts [2], [16], [13].

B. Aberration-Aware Placement Formulation

We now propose a novel aberration-aware timing-driven placement objective for improved timing yield after manufacturing, and describe its integration into the analytical placement framework. We perform aberration-aware timing-driven placement by optimizing a hybrid placement objective. Besides the typical objective of minimizing total timing-weighted net wirelength, we also minimize the sum of timing-weighted delays of timing-critical cells. The aberration-aware timing-driven placement formulation is as follows:

$$\begin{aligned} min \quad & WWL(\mathbf{x},\mathbf{y}) + W_a \sum_v w(v) \cdot g_{t_v}(x_v) \\ s.t. \quad & D_g(\mathbf{x},\mathbf{y}) = D \text{ for each global cell } g \\ & \text{and } g_{t_v}(x_v) = MAX\{g^1 t_v(x_v), \cdots, g^n t_v(x_v)\} \end{aligned} \quad (3)$$

where $WWL(\mathbf{x},\mathbf{y})$ is the sum of timing-weighted net HPWL of the current placement and W_a is the weight for the aberration-aware timing-driven objective function terms, which is the sum of timing-weighted delays of timing-critical cells. In the formulation, $g_{t_v}(x_v)$ is the delay function, obtained TTL timing library from the described above, for cell instance v's timing model t_v; it is a function of v's horizontal position x_v in the chip. In the situation that there are multiple copies ($n > 1$) of chips in the reticle, we let $g^i t_v(x_v)$ be the delay function for the ith chip, and we consider the maximum delay of cell instance v over all copies so that the performance of the slowest chips is improved.

As with traditional net weighting methods, we assign timing weights to cells based on timing criticality and path sharing. First, a cell along a timing-critical path should receive a heavy weight. Second, a cell with many timing-critical paths passing through should have a large weight as well. Therefore, we assign to cell v the weight $w(v)$.

$$w(v) = \sum_{v \in \pi} (D_s(slack_s(\pi), T_s) \cdot D_h(slack_h(\pi), T_h) - 1) \quad (4)$$

where

$$D_s(s,T) = \begin{cases} (1 - s/T)^{\delta} & s \leq 0 \\ 1 & s \geq 0 \end{cases} \quad (5)$$

and

$$D_h(s,T) = \begin{cases} (1 + s/T)^{\delta} & s \leq 0 \\ 1 & s \geq 0 \end{cases} \quad (6)$$

Here, δ is the criticality exponent, and u is the expected improvement of the longest (or shortest) path delay after this timing-driven iteration. T is $T_s = (1-u) \cdot \max_{\pi}\{delay(\pi)\}$ for setup-critical paths or $T_h = (1+u) \cdot \min_{\pi}\{delay(\pi)\}$ for hold-critical paths. Additionally, $slack_s(\pi) = T_s - delay(\pi)$ is the slack of a setup-critical path π and $slack_h(\pi) = delay(\pi) - T_h$ is the slack of a hold-critical path π. In Equation (4), we compute a weight for each timing-critical path based on its slack and obtain the timing weight of a cell by summing up the weights of timing-critical paths passing

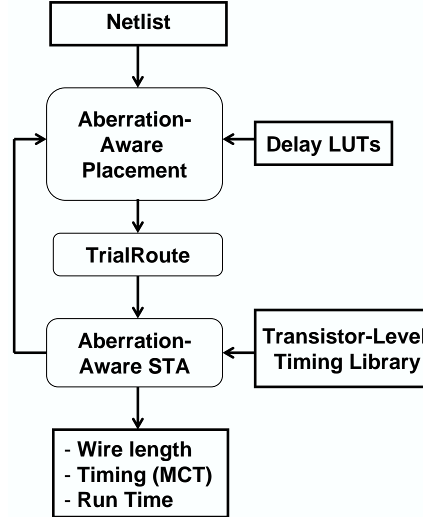

Fig. 9. Aberration-aware timing-driven placement and evaluation flow.

through it. Note that similar functions have been previously applied to assign timing weights to nets for timing-driven layout [18], [17], [12].

C. Placement Flow

Our aberration-aware timing-driven placement and evaluation flow is shown in Figure 9. Besides the design netlist, inputs to the aberration-aware placer also include the above-described delay functions, g_{t_v}, of cell models, which represent how the delays of given cell models change with horizontal position in the chip.

The timing-driven process in our placer may include several iterations. As shown in Figure 9, during each iteration, we send the intermediate placement to *TrialRoute* (*Cadence First Encounter* v04.10) to perform a fast global and detailed routing, and extract RC parasitics. We then change the type of each cell in the netlist according to its horizontal position within the lens field and use a commercial tool, *Synopsys PrimeTime* (version W-2004.12-SP2) to perform accurate aberration-aware Static Timing Analysis (STA) with the transistor-level timing libraries (TTLs) described in Section 3. The resulting critical paths are imported into the placer to decide timing weights for nets and cells. The total timing-weighted cell delay is then minimized using the Conjugate Gradient solver, together with the timing-weighted wirelength objective, and subject to density constraints.

D. Implementation Details

We compute the weight of the aberration-aware objective W_a in Equation (3) according to the x-gradients derived from the wirelength and delay terms so that the scaled gradients of delay functions are comparable to the wirelength gradients:

$$W_a = \alpha \cdot (\sum_v |\frac{\partial WWL}{\partial x_v}|) \ / \ (\sum_v |\frac{\partial g_{t_v}}{\partial x_v}|) \tag{7}$$

where the delay ratio α decides the ratio of the delay gradients to the wirelength gradients, and needs to be carefully tuned according to the impact of reduced cell delay and increased net wirelength on design performance.

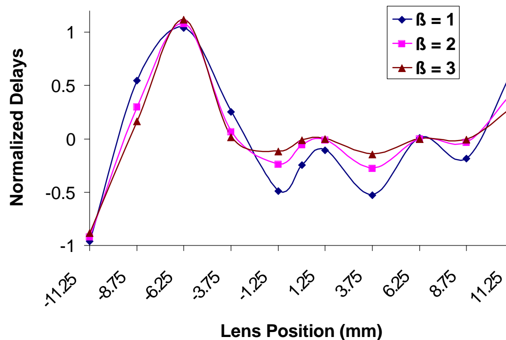

Fig. 10. Delay curves of NOR2X1 with a variety of smoothing factors (β's).

Design	Utilization (%)	Chip Side (mm)	#Cells	#Nets
AES	60	0.50	17304	17465
JPEG	60	1.41	118321	125036

TABLE I

DESIGN CHARACTERISTICS OF TWO BENCHMARK CIRCUITS.

We derive the delay of a cell at a specific horizontal field position by averaging the rising and fall delays of all timing arcs with zero wire load, according to the transistor-level timing libraries. Therefore, the delay functions represent how gate delays vary with horizontal locations and gate CDs. Due to simulation limits, delay functions only have accurate values at discrete horizontal coordinates, and thus are expressed as look-up tables (LUTs). We obtain delay at continuous positions using linear interpolation and compute gradients accordingly.

A smoothing technique [8] can be applied to smooth the delay curves and avoid local minimums. Given a normalized delay function, a smooth function is given by a pre-defined smoothing factor β (≥ 1) as follows:

$$g' = \begin{cases} \overline{g} + (g - \overline{g})^{\beta} & if\ g \geq \overline{g} \\ \overline{g} - (\overline{g} - g)^{\beta} & if\ g \leq \overline{g} \end{cases} \tag{8}$$

where $\overline{g}$ is the average value of the delay function. Figure 10 shows the delay curves with a variety of smoothing factors β's for NOR2X1. A delay function generated from a larger β exhibits a smoother curve, and a delay function generated from a smaller β exhibits a more rugged curve.

V. EXPERIMENTS

In this section, we empirically test our approach on two real designs within a standard industry flow using leading-edge tools. We measure impacts on timing, wirelength and runtime.

Experimental Setup. We use two designs from *OpenCores* [27] as our testcases. The circuits are synthesized using

Design	Method	Place		TrialRoute		STA
		HPWL (e9)	CPU (s)	WL (e5)	#Vias	MCT (ns)
AES	APlace_WL	1.032	631	6.183	1.128	1.67
	AberrPl_WL	1.063	616	6.269	1.174	1.59
	Impr. (%)	**-3.01**	**2.34**	**-1.39**	**-4.12**	**4.66**
	APlace_TD	1.054	672	6.258	1.129	3.85
	AberrPl_TD	1.082	654	6.411	1.127	3.53
	Impr. (%)	**-2.68**	**2.75**	**-2.44**	**0.08**	**8.38**
JPEG	APlace_WL	10.604	3620	5.891	7.531	2.54
	AberrPl_WL	10.727	3844	5.966	7.576	2.44
	Impr. (%)	**-1.16**	**-6.19**	**-1.27**	**-0.59**	**4.24**
	APlace_TD	10.665	3755	5.915	7.555	10.86
	AberrPl_TD	10.822	3967	6.013	7.623	9.79
	Impr. (%)	**-1.47**	**-5.64**	**-1.66**	**-0.90**	**9.80**

TABLE II

COMPARISON OF ABERRATION-AWARE PLACEMENT VERSUS TRADITIONAL WIRELENGTH- OR TIMING-DRIVEN PLACEMENT FOR AES AND JPEG.

Synopsys Design Compiler (version W-2004.12-SP3) with tight timing constraints and a set of 63 most commonly used cell models in Artisan TSMC 90nm library, then floorplanned in *Cadence First Encounter* (v04.10). The design characteristics are summarized in Table I.

The experimental flow is shown in Figure 9. The inputs for each design include technology libraries, synthesized netlists, floorplan, timing constraints, aberration-aware timing libraries, and delay look-up tables. For each design, our aberration-aware timing-driven placer, *AberrPl*, is applied to perform two placement runs: (1) with pure HPWL objective and no RC extraction before timing analysis (AberrPl_WL) and (2) with timing-driven wirelength objective and RC extraction before timing analysis (AberrPl_TD). Comparing with the placement runs by wirelength-driven APlace (APlace_WL) and timing-driven APlace (APlace_TD) respectively, we show how much our aberration-aware timing-driven objective improves chip performance, without and with traditional timing-driven wirelength objective and/or interconnect load and delay during timing analysis.

Intuitively, chips with large sizes will benefit more from our aberration-aware placement technique, since there is larger CD and delay variation induced by an imperfect lens system across the layout region. However, available testcases are not large enough to clearly show the effect of lens aberration. We illustrate the aberration effects and show the effectiveness of our method by scaling the CD and delay functions along the horizontal direction to control the amount of variation within the layout region.

For the aberration-aware placement runs, unless otherwise noted, we will compute timing weights with a criticality exponent $\delta = 4$ and expected improvement $u = 10\%$, and assume that "there is only one copy of the chip within the lens field" with scaling.

After each placement, we perform a fast global and detailed routing, RC extraction and finally aberration-aware timing analysis using PrimeTime. Minimum cycle time (MCT) of the slowest chip in the reticle is reported by the

AberrPl_WL								
Ratio	**Place**			**TrialRoute**			**AberrSTA**	
	HPWL		**CPU**	**WL**		**#Vias**	**MCT**	
	(e9)	**(%)**	**(s)**	**(e5um)**	**(%)**		**(ns)**	**(%)**
0.000	1.032	0.00	631	6.183	0.00	1.128	1.67	0.00
0.025	1.024	0.75	613	6.111	1.16	1.143	1.65	1.20
0.050	1.021	1.06	608	6.080	1.67	1.153	1.62	3.00
0.075	1.049	-1.66	626	6.235	-0.84	1.155	1.61	3.52
0.100	1.040	-0.80	629	6.157	0.42	1.169	1.59	4.27
0.125	1.054	-2.18	621	6.228	-0.73	1.173	1.59	4.57
0.150	1.063	-3.01	616	6.269	-1.39	1.174	1.59	4.66
0.175	1.065	-3.19	611	6.282	-1.60	1.174	1.59	4.65
0.200	1.108	-7.37	623	6.522	-5.48	1.179	1.59	4.65
0.225	1.101	-6.70	622	6.474	-4.71	1.182	1.59	4.65
AberrPl_TD								
Ratio	**Place**			**TrialRoute**			**AberrSTA**	
	HPWL		**CPU**	**WL**		**#Vias**	**MCT**	
	(e9)	**(%)**	**(s)**	**(e5um)**	**(%)**		**(ns)**	**(%)**
0.000	1.054	0.00	672	6.258	0.00	1.129	3.85	0.00
0.025	1.069	-1.44	654	6.344	-1.37	1.124	3.59	6.93
0.050	1.068	-1.33	643	6.336	-1.25	1.127	3.57	7.46
0.075	1.082	-2.68	654	6.411	-2.44	1.127	3.53	8.38
0.100	1.096	-4.01	638	6.477	-3.50	1.129	3.90	-1.28
0.125	1.094	-3.81	684	6.454	-3.13	1.135	4.06	-5.40
0.150	1.084	-2.87	648	6.402	-2.30	1.136	4.04	-4.73
0.175	1.140	-8.14	686	6.696	-7.00	1.135	3.89	-1.02
0.200	1.101	-4.42	626	6.495	-3.79	1.135	4.08	-5.73
0.225	1.164	-10.42	691	6.808	-8.79	1.160	3.43	10.96

TABLE III

RESULTS OF ABERRATION-AWARE PLACEMENTS (ABERRPL_WL AND ABERRPL_TD) WITH A VARIETY OF DELAY RATIOS (β'S) FOR CIRCUIT AES.

aberration-aware STA to measure performance of timing-driven placements; we also report HPWL and runtime (minutes) from placement, and routed wirelength and the number of vias of TrialRoute's results. All the experiments are performed on Linux machines with 2.4GHz CPUs and 4GB memory.

Experimental Results. Table II summarizes the results of AberrPl_WL and AberrPl_TD for AES and JPEG. According to the results, AberrPl_WL reduces MCT by 4.7% with 3.0% HPWL increase and 1.4% increase of trial-routed wirelength for AES, and reduces MCT by 4.2% with 1.2% HPWL increase and 1.3% increase of trial-routed wirelength for JPEG. When combined with the traditional timing-driven placement method, our aberration-aware placer (AberrPl_TD) reduces MCT by 8.4% with 2.7% HPWL increase and 2.4% increase of trial-routed wirelength for AES, and reduces MCT by 9.8% with 1.5% HPWL increase and 1.7% increase of trial-routed wirelength for JPEG.

Impact of Delay Ratio. The second set of experiments are performed for circuit AES with a variety of delay ratios

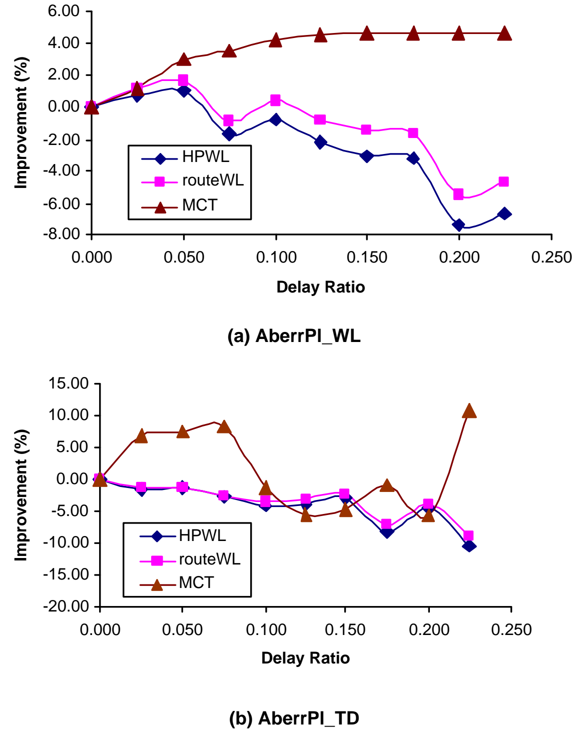

Fig. 11. MCT, HPWL and routed wirelength of AberrPl_WL and AberrPl_TD as functions of delay ratio (α) for circuit AES.

(α's) ranging from 0 to 0.225 in steps of 0.025. The results are summarized in Table III. For each delay ratio, we perform aberration-aware placements using AberrPl_WL and AberrPl_TD, and compare the results to the reference runs of APlace_WL and APlace_TD. Note that during each timing iteration we assign a set of timing weights to nets and cells according to the current placement. This makes the analytical placement unsteady, since the placement objective keeps changing. Therefore, here we only apply small delay ratios in order to reduce the instability of the placements.

The results of AberrPl_WL clearly show the performance improvements obtained using our aberration-aware placement method. According to the first part of Table III, our aberration-aware placer can reduce MCT by 4.7% with 3.0% HPWL increase and 1.4% increase of trial-routed wirelength. Figure 11(a) shows the curves of MCT, HPWL and routed wirelength impacts of AberrPl_WL as functions of delay ratio. We see that MCT improvement generally increases with delay ratio to 4.7% when $\alpha = 0.150$, with wirelengths generally increasing.

When combined with the traditional timing-driven placement method, AberrPl_TD achieves an MCT reduction of 8.4% when $\alpha = 0.075$ with 2.7% increase of placed HPWL and 2.4% increase of trial routed wirelength, according to the second part of Table III. However, since timing analysis is very sensitive to the actual placement with wire load considered, it in turn increases the instability of timing weights and hence placement results. Therefore, we see a very unsteady curve of MCT in Figure 11(b); inferences from this data are not quite clear.

Impact of Scaling. A third set of experiments are designed to show the effect of chip size on performance improvement obtained with our aberration-aware placement method. We perform aberration-aware placements for circuit AES

Copies	Method	Place		TrialRoute		AberrSTA
		HPWL (e9)	**CPU (s)**	**WL (e5um)**	**#vias (e5)**	**MCT (ns)**
1	APlace_WL	1.032	631	6.183	1.128	1.67
	AberrPl_WL	1.063	616	6.269	1.174	1.59
	Imp (%)	**-3.01**	**2.34**	**-1.39**	**-4.12**	**4.66**
2	APlace_WL	1.032	631	6.183	1.128	1.70
	AberrPl_WL	1.061	644	6.289	1.167	1.65
	Imp (%)	**-2.83**	**-2.12**	**-1.71**	**-3.45**	**2.91**
4	APlace_WL	1.032	631	6.183	1.128	1.70
	AberrPl_WL	1.061	642	6.291	1.166	1.69
	Imp (%)	**-2.88**	**-1.74**	**-1.75**	**-3.37**	**0.83**
6	APlace_WL	1.032	631	6.183	1.128	1.69
	AberrPl_WL	1.054	663	6.260	1.163	1.68
	Imp (%)	**-2.16**	**-5.15**	**-1.25**	**-3.12**	**0.24**
8	APlace_WL	1.032	631	6.183	1.128	1.70
	AberrPl_WL	1.056	673	6.279	1.153	1.70
	Imp (%)	**-2.38**	**-6.71**	**-1.55**	**-2.25**	**0.16**

TABLE IV

RESULTS OF ABERRATION-AWARE PLACEMENTS (ABERRPL_WL) WITH A VARIETY OF SCALING FACTORS FOR CIRCUIT AES.

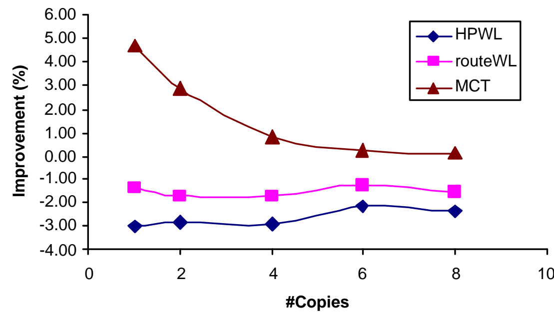

Fig. 12. MCT, HPWL and routed wirelength of AberrPl_WL as functions of the scaling factor for circuit AES.

using AberrPl_WL with delay ratio of 0.15 and a variety of scaling factors, such that the number of die copies within the reticle is 1x1, 2x2, 4x4, 6x6, and 8x8. The results are summarized in Table IV. Figure 12 shows the curves of MCT, HPWL and routed wirelength impacts as functions of the scaling factor. We see that the performance improvement obtained decreases with the number of copies in the field. When the chip size is small, although there is a significant CD and delay variation across the reticle, the variations within the layout area are too small to achieve any benefit from aberration-aware placement methods.

VI. CONCLUSION AND ONGOING WORK

We have proposed an accurate aberration-aware timing analysis flow and a novel aberration-aware timing-driven placement technique, *AberrPl*, as a practical and effective approach to improve timing yield after manufacturing. We

implement our method based on a general analytical placement framework and test it within a standard industry flow using leading-edge tools. For two benchmark designs in 90nm technology, AberrPl achieves an average improvement of $\sim$ 5% in minimum clock cycle time with a wirelength increase of $\sim$ 2% on average. The benefits of AberrPl are expected to increase in future technology nodes. We are currently engaged in further experimental validation and research. Our ongoing research is in the following directions.

- The proposed aberration-aware placement approach aims at improving performance of all design, copies in the field and hence is limited by the slowest ones. However, for many designs chips of slower speeds can also be sold, albeit at a lower value (speed binning). We plan to improve our approach so that the total value of all chips is maximized.
- We also wish to enhance our placer to comprehend leakage constraints, since leakage is increasingly starting to determine yield and is exponentially affected by CD.
- We are developing an aberration-aware OPC method which applies different OPC models for devices at different lens positions, instead of the simple OPC method with average Zernike coefficients across the reticle, to improve pattern printability and lithographic process window.
- Restricted design rules have been receiving increased attention from industry. E.g., relaxed pitch helps to reduce CD asymmetry caused by coma aberration. We intend to compare such approaches with AberrPl in terms of design and manufacturability metrics.

We are very grateful to Advanced Micro Devices for discussions of CD impact of lens aberration. We also thank Artisan Components (ARM Holdings, PLC) for access to library data used in our research.

References

[1] T.A. Brunner, "Impact of Lens Aberrations on Optical Lithography", *IBM Journal of Research and Development* (41) (1997). `http://www.research.ibm.com/journal/rd/411/brunner.html`.

[2] Y.-S. Cheon, P.-H. Ho, A. B. Kahng, S. Reda and Q. Wang, "Power-Aware Placement", *Proc. Design Automation Conference*, 2005, pp. 795-800.

[3] H. Eisenmann and F. M. Johannes, "Generic Global Placement and Floorplanning", *Proc. Design Automation Conf.*, 1998, pp. 269-274.

[4] H. Etawil, S. Areibi and A. Vannelli, "Attractor-Repeller Approach For Global Placement", *Proc. Int. Conf. Computer Aided Design*, 1999, pp. 20-24.

[5] D. G. Flagello, H. Laan, J. Schoot, I. Bouchoms, and B. Geha, "Understanding Systematic and Random CD variations using Predictive Modelling Techniques", *Proc. SPIE* 3679 (1999), pp. 162-175.

[6] N. Farrar, A. Smith, D. Busath, and D. Taitano, "In-Situ Measurement of Lens Aberrations", *Proc. SPIE* 4343 (2001), pp. 18-29.

[7] J. Gortych and D. Williamson, "Effects of Higher-Order Aberrations on the Process Window," *Proc. SPIE* 1463 (1991), pp. 368-381.

[8] J. Gu and X. Huang, "Efficient Local Search with Search Space Smoothing: A Case Study of the Traveling Salesman Problem (TSP)," *IEEE Trans. Systems, Man and Cybernetics* 24(5) (1994), pp. 728-735.

[9] B. Hu and M. Marek-Sadowska, "FAR: Fixed-Points Addition & Relaxation Based Placement", *Proc. Int. Symp. Physical Design*, 2002, pp. 161-166.

[10] A. B. Kahng C.-H. Park, P. Sharma and Q. Wang, "Lens Aberration Aware Timing-Driven Placement", *Proc. Design Automation and Testing in Europe*, 2006 to appear.

[11] A. B. Kahng and Q. Wang, "Implementation and Extensibility of an Analytic Placer", *Proc. Int. Symp. Physical Design*, 2004, pp. 18-25.

[12] A. B. Kahng and Q. Wang, "An Analytic Placer for Mixed-Size Placement and Timing-Driven Placement," in *Proc. IEEE International Conference on Computer Aided Design*, 2004, pp. 565-572.

[13] A. B. Kahng and Q. Wang, "Implementation and Extensibility of an Analytic Placer," *IEEE Transactions on Computer-Aided Design* 24(5) (2005), pp. 734-747.

[14] A. B. Kahng, S. Reda, and Q. Wang, "APlace: A General Analytic Placement Framework," in *Proc. ACM/IEEE International Symposium on Physical Design*, 2005, pp. 233-235.

[15] A. B. Kahng, S. Reda, and Q. Wang, "Architecture and Details of a High Quality, Large-Scale Analytical Placer," in *Proc. Int. Conf. Computer Aided Design*, 2005, to appear.

[16] A. B. Kahng, B. Liu, and Q. Wang, "Supply Voltage Degradation Aware Analytical Placement," in *Proc. ACM/IEEE Intl. Conf. on Computer-Aided Design*, 2005, pp. 437-443.

[17] T. Kong, "A Novel Net Weighting Algorithm for Timing-Driven Placement", *Proc. Int. Conf. Computer Aided Design*, 2002, pp. 10-14.

[18] A. Marquardt, V. Betz and J. Rose, "Timing-Driven Placement for FPGAs", *Proc. ACM Symp. FPGAs*, 2000, pp. 203-213.

[19] T. Matsuyama, Y. Shibazaki, Y. Ohmura, and T. Suzuki, "High NA and Low Residual Aberration Projection Lens for DUV Scanner", *Proc. SPIE* 1491 (2002), pp. 687-695.

[20] W. Naylor et al., "Non-Linear Optimization System and Method for Wire Length and Delay Optimization for an Automatic Electric Circuit Placer", *US Patent* 6301693, Oct. 2001.

[21] C.-H. Park et al., "Hybrid PPC Method Based on the Emperical Etch Model for the 0.14μm DRAM Generation and Beyond", *IEEE ISQED*, 2002, pp. 143-139.

[22] C. J. Progler, A. Borna, D. Blaauw and P. Sixt, "Impact of Lithography Variability on Statistical Timing Behavior", *Proc. Design and Process Integration for Microelectronic Manufacturing II*, SPIE Vol. 5379, May 2004, pp. 101-110.

[23] M. Orshansky, L. Milor, L. Nguyen, G. Hill, Y. Peng and C. Hu, "Intra-Field Gate CD Variability and Its Impact on Circuit Performance", *IEDM Technical Digest* (1999), pp. 479-482.

[24] M. Orshansky, L. Milnor, P. Chen, K. Keutzer and C. Hu, "Impact of Spatial Intrachip Gate Length Variability on the Performance of High-Speed Digital Circuits," *IEEE Transactions on Computer-Aided Design of Integrated Circuits and Systems* 21(5) (2002), pp. 544-553.

[25] M. Orshansky, L. Milnor, P. Chen, K. Keutzer and C. Hu, "Impact of Spatial Intrachip Gate Length Variability on the Performance of High-Speed Digital Circuits," *IEEE Transactions on Computer-Aided Design of Integrated Circuits and Systems* 21(5) (2002), pp. 544-553.

[26] M. Orshansky, L. Milor and C. Hu, "Characterization of Spatial Intrafield Gate CD Variability, Its Impact on Circuit Performance, and Spatial Mask-Level Correction," *IEEE Transactions on Semiconductor Manufacturing* 17(1) (2004), pp. 2-11.

[27] http://www.opencores.org/

[28] Y. Shiode, S. Okada, H. Takamori, H. Matusda and S. Fujiwara, "Method of Zernike Coefficients Extraction for Optics Aberration Measurement", *Proc. SPIE* 1491 (2002), pp. 138-147.

[29] K. K. H. Toh and A. Neureuther, "Identifying and Monitoring Effects of Lens Aberrations in Projection Printing," *Proc. SPIE* 772 (1987), pp. 202-209.

[30] N. Viswanathan and C. C.-N. Chu, "FastPlace: Efficient Analytical Placement Using Cell Shifting, Iterative Local Refinement and a Hybrid Net Model", *Proc. Int. Symp. Physical Design*, 2004, pp. 26-33.

[31] A. K. Wong, "Theoretical Discussion on Reduced Aberration Sensitivity of Enhanced Alternating Phase-Shifting Masks", *Proc. SPIE* 14691 (2002), pp. 395-368.

[32] A. K. Wong, "Resolution Enhancement Techniques in Optical Lithography ", SPIE PRESS Vol. TT47 (2001).